Run-out of landslides in brittle soils

A. Yerro[1] & E.E. Alonso[1,2] & N.M. Pinyol[1,2]
[1]*Department of Geotechnical Engineering and Geosciences, UPC, Barcelona, Spain*
[2]*Centre Internacional de Mètodes Numèrics en Enginyeria*

ABSTRACT: One of the factors causing the acceleration of landslides is the loss of strength of the soil involved in the potential unstable mechanism. The travelled distance and the landslide velocity, a key factor in risk analysis, will be determined by the loss of resistant forces. Brittle behaviour, commonly associated with cemented soils, overconsolidated plastic clay formations and sensitive clays, lead to the progressive failure phenomenon explained by the reduction of the strength with increasing strain. In the present study, this phenomenon has been analysed in the case of a saturated slope which becomes unstable by increasing the boundary pore water pressure. A Mohr-Coulomb model with strain softening behaviour induced by increasing deviatoric plastic strain is used. The paper focusses not only on the stability of the slope but also on the post failure behaviour (run-out and sliding velocity). A coupled hydro-mechanical formulation of the Material Point Method has been used to simulate the whole instability process. The influence of the brittleness of the material on the triggering of instability and run-out is evaluated by means of a parametric study varying peak and residual strength. The onset of the failure and the failure geometry are controlled by both peak and residual values. Good correlations between run-outs and brittleness are found. The decay of the strength determines the acceleration of the landslides and the travelled distance.

1 INTRODUCTION

The dynamic behaviour of landslides receives increasing attention because landslide risk analysis and spatial identification of vulnerable areas require estimations of the slide run-out and the velocity of the unstable mass [1]. Special attention is given to reservoirs, lakes and fjords potentially affected by landslides on their margins [2–4]. In fact, slope instabilities may affect dams and their foundations and they may lead to partial or complete blockage of rivers, creating dangerous “natural” dams or the generation of a destructive wave due to the impact of the landslide against the stored water [5–7]. The potential damage caused by landslides can be determined by several factors related with the volume of the mobilized mass, the run-out, velocity and acceleration. One of the factors that control the acceleration of the slide is the loss of resistant forces associated with the drop of available soil strength. This phenomenon is typically observed in first time failure developed in “intact” sites in materials exhibiting a brittle behaviour. This is the case of hard soils and soft rocks, overconsolidated and cemented clayey

soils with special relevance in the case of high plasticity soils. These materials exhibit a softening behaviour from a peak value, associated with a low value of shearing displacements, to a low residual strength when bonds are destroyed and clay particles orient in the direction of shearing. This reduction of strength leads to the propagation of the failure surface following a process of progressive failure.

When a point exceeds the maximum available strength, a degradation process initiates due to the strain softening associated with the constitutive response of the material. The unbalanced stresses are transferred to the surrounding areas which in turn may overstress neighbouring points in the process, leading eventually to residual strength conditions. This stress transfer phenomenon develops during slip surface propagation. This mechanism was first recognized by Terzaghi and Peck [8] and Taylor [9]. It was further discussed in the context of overconsolidated clays and clay shales by Skempton [10], Bjerrum [11] and Bishop [12]. Further contribution are made by Palmer and Rice [13], Stark and Eid [14], and Puzrin and Germanovich [15].

Several real cases involving progressive failure are collected and analyzed in the literature [16–20]. Troncone [21] presents a 2D numerical analysis of well documented Senise large landslides in Southern Italy and a 3D extension in [22]. Other real cases of landslides involving progressive failure mechanism in the Iberian Peninsula have been collected in [23].

Contributions mentioned above mainly concentrate on the analysis of the generation and evolution of the failure surface but the run-out stage, once instability occurs, is not explored. Modelling large displacement involves the use of alternative calculation techniques to the Lagranian approaches generally used in FEM. Soga et al. [24] reviews current numerical methods capable of analysing the slide motion. In this work, the Material Point Method (MPM) [25] is selected to analyse the stability of slopes and their post failure response in strain softening materials. MPM is a numerical technique able to simulate large displacements by means of combining two discretizations of the media: (a) a set of material points which move through (b) a fixed computational grid. This dual description prevents mesh distortion problems and contacts between different bodies are automatically solved.

A fully coupled hydro-mechanical material point code was developed for saturated soils within the MPM Research Community framework [26–29]. A strain softening elastoplastic constitutive law was has been implemented with the purpose of analysing progressive failure phenomena that take place in materials exhibiting a reduction of the strength with increasing strain [30].

This MPM formulation was recently applied in Alonso et al. [31] to model the Selborne failure experiment [32]. Failure of the Selborne slope was triggered by forced water recharge. Field

instrumentation data indicated that the failure was a progressive mechanism in overconsolidated brittle clays. The numerical MPM analysis presented in [31] provided consistent and accurate results in the prediction of the shape and position of the failure surface, the development of progressive failure and the slide motion after failure.

The aim of the paper is to explore the response of saturated slopes in brittle materials. It focusses on exploring the material properties controlling the run-out distance and velocity of the unstable mass in brittle materials. First, a synthetic slope is presented in which the shear stress distribution and the progression of failure mechanism are discussed. Afterwards, by means a parametric analysis, the brittle behaviour of the material soil (defined in terms of brittleness index I_B) is shown to be a key factor of the slope response. The results are discussed with the aim of deriving practical conclusions.

2 BASIS OF MPM FORMULATION

The MPM [33] discretizes the continuum as a set of subdomains. In the standard approach, presented by Sulsky et al. [25], the mass of each subdomain is considered to be concentrated in a point, the material point (Fig. 1). Other properties such as velocities, strains and stresses, are also carried by the material points. This information is projected on to a background mesh where governing equation are solved. The support computational mesh covers the full domain of the problem and remains fixed during calculation. Calculations on the mesh serve to update the material point properties and location. Linear interpolation shape functions are used to provide the relationship between material points and nodes at any point of the domain. This approach allows MPM to combine the advantages of Eulerian and Lagrangian formulations.

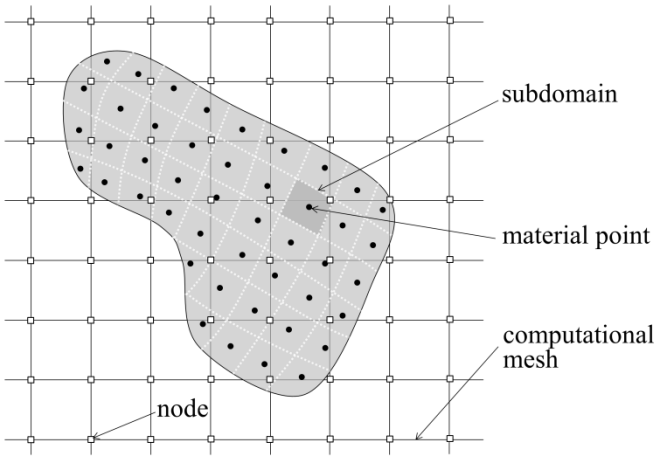

Fig. 1. Scheme of the spatial discretization used in MPM formulation.

The MPM formulation for a mechanical problem was presented by Sulsky and Schryer [34]. Different authors have extended the MPM to solve coupled hydro-mechanical problems under saturated conditions [20,27,35]. More recently, Yerro et al. [28] extended MPM for unsaturated soils.

The numerical approach considered in this work to simulate saturated soils is based on [27]. It assumes that each material point represents a portion of the soil, moves attached to the solid skeleton and carries information of solid and liquid phases. Solid and liquid accelerations are calculated in the computational mesh solving the dynamic momentum balances of both phases. Velocities, displacements and strains are obtained in the material points; and liquid mass balance equation is established in the material points to provide liquid pressures. An explicit Euler-Cromer scheme [36] is used to update displacements and velocities from calculated accelerations.

In order to avoid non-physical vibrations, it is common to include a damping term in the balance equations. The approach adopted here was presented by Cundall [37]. It introduces a damping force proportional to the corresponding out-of-balance force (proportional factor α) and opposite to the phase velocity. In dynamic problems, the proportional factor should be very small (0-5%) in order to approximate the correct solution and avoid an overdamped system.

The standard MPM approach [25,33] in which the mass of each material point is assumed to be concentrated at the corresponding material point, suffers from spurious oscillations when material points cross from one element to another one. It is caused by a jump discontinuity in the gradient of low-order shape functions that are used for the integration. In order to reduce this numerical problem, a simple technique of low computational cost is introduced in this work [38]. It arises from considering that the stress on each element is constant and corresponds to the average of the stresses of the material points located within a given cell. Other authors proposed more accurate techniques. For instance, Bardenhagen and Kober [39] proposed to distribute the mass of each material point in a certain region. This idea results in a family of methods known as Generalized Interpolation Material Point (GIMP) methods. More recently, MPM has been extended to convected particle domain interpolation methods (CPDI1 and CPDI2) which are developed to improve the tracking of material point domains [40,41].

3 CONSTITUTIVE MODELLING

In this paper the basic non-associated Mohr-Coulomb law is generalized to introduce strain softening plasticity with the aim of modelling a strength loss after peak strength conditions. In order to reduce the singularities of Mohr-Coulomb yield surface (edges and tip) that involve

some numerical problems during the elasto-plastic integration, the modifications proposed by Abbo and Sloan [42] have been implemented.

Following previous contributions [43–47], the softening behaviour is accounted for by reducing the strength parameters (friction angle φ', and cohesion c') exponentially with the accumulated deviatoric plastic strain ε_d^p according to the following softening rules:

$$c' = c'_r + \left(c'_p - c'_r\right) e^{-\eta \varepsilon_d^p} \tag{2}$$

$$\phi' = \phi'_r + \left(\phi'_p - \phi'_r\right) e^{-\eta \varepsilon_d^p} \tag{3}$$

The deviatoric plastic strain invariant is defined as:

$$\varepsilon_d^p = \sqrt{\frac{2}{3}\mathbf{e}_{ij}^p \mathbf{e}_{ij}^p} \tag{4}$$

where $\mathbf{e}_{ij}^p$ is the deviatoric part of the plastic strain tensor.

The model requires the specification of peak (c_p',φ_p') and residual (c_r',φ_r') effective strength parameters. An additional parameter η, a shape factor parameter, is also necessary in order to control the rate of strength decrease.

The effect of η in a simple shear test simulation is shown in Fig. 2. The soil parameters of the material considered in these simulations are summarised in Table 1. A vertical stress of 50 kPa and a horizontal one of 25 kPa are applied to confine the sample. Then, a prescribed velocity is imposed at the upper boundary maintaining the bottom fixed. High values of η lead to faster degradation of the soil strength.

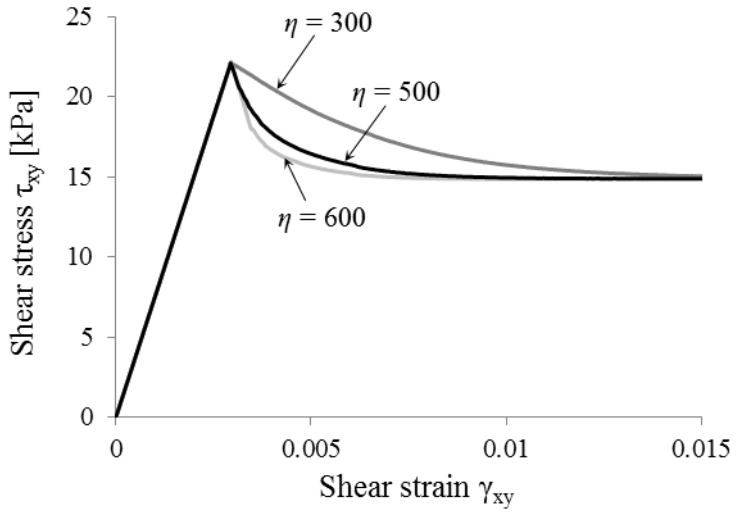

Fig. 2. Evolution of shear stress in a numerical model of a simple shear tests for different values of parameter η.

4 A REFERENCE SLOPE INSTABILITY PROBLEM

The instability of a synthetic slope, 6 m high and 37º steep, was analysed (Fig. 3). The slope failure was triggered by increasing the pore water pressure at the lower boundary simulating a phreatic level rise. This is a plane strain simulation in which the boundary conditions on the vertical contours are rollers and the base is fixed. The water pressure is zero along the slope surface, the lateral contours are impermeable and saturated conditions are considered during the calculation. The mesh was refined in the region where the failure is expected in order to get more accurate results and to optimise the computational cost.

Initially the slope remains in equilibrium. The calculation starts with the application of a 40 kPa increase in pore pressure (ΔP) along the lower boundary during 1 second. Afterwards the water pressure on the boundary is maintained constant during the entire simulation.

The Mohr-Coulomb strain softening model described in the previous section was used to simulate the brittle behaviour of a soil. The properties of the slope material are given in Table 1. The particular values selected are not relevant for the discussion presented here. The only requirement to select such values has been to ensure that the failure occurs for the imposed increment of pore water pressure. The effect of the shape factor parameter on the drop of the strength is shown in Fig. 2.

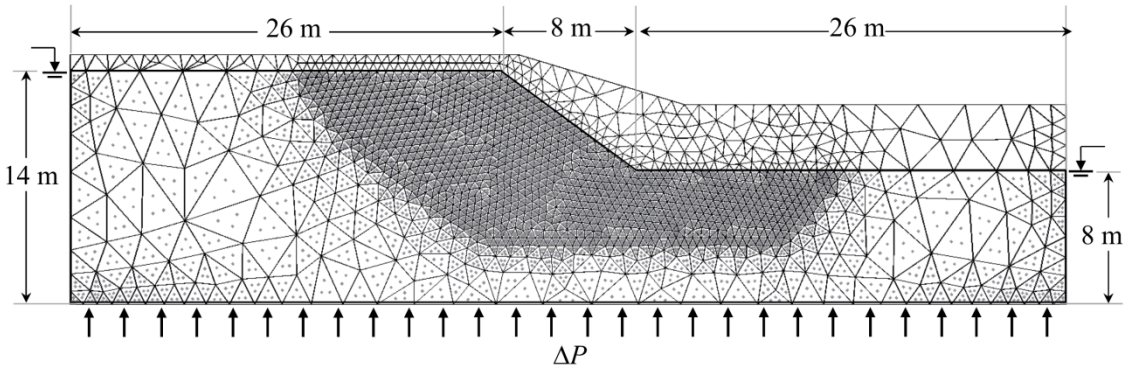

Fig. 3. Scheme of the MPM model. Initial distribution of the material points and computational mesh.

Table 1. Soil parameters of the slope.

Soil parameters	*Value*
Porosity [-]	0.2
Intrinsic permeability [m^2]	10^{-10}
Young's modulus [kPa]	20000
Poisson's ratio [-]	0.33
Peak cohesion [kPa]	5
Residual cohesion [kPa]	0.5
Peak friction angle [º]	35
Residual friction angle [º]	20
Shape factor parameter	500
Dilatancy angle [º]	0

An explicit Euler-Cromer scheme is used to discretise the governing equations. Because it is conditionally stable, very small time steps are required in the calculation. Since permeability is not a relevant parameter in the analysis presented here, a high value (0.001 m/s) has been adopted to simulate the slope failure in a relatively short time.

In order to reduce numerical instabilities a damping force has been included in the momentum balance equation. It is proportional to the corresponding unbalanced force by means a proportional factor $\alpha = 0.05$.

The increase of pore pressure reduces the effective stresses in the slope leading some points to reaching peak conditions. The strain softening effect decreases progressively the strength parameters of the plastic zones down to the residual yield surface. As a result, the gravitational stresses are sufficient to induce a progressive failure in the case analysed.

Failure development is illustrated in Fig. 4 by representing the shear strain contours at two different times. At 8.3 s a shear band localises providing a failure mechanism and afterwards the instability initiates. During the movement, the shear band spreads. Finally, when the new geometry becomes stable, a wider shear zone is observed (Fig. 4b). Fig. 5 shows the final

displacements field. In this case, the achieved maximum displacement is 9.1 m and the displacement between the toe of the initial and the final slope geometries is 9.5 m.

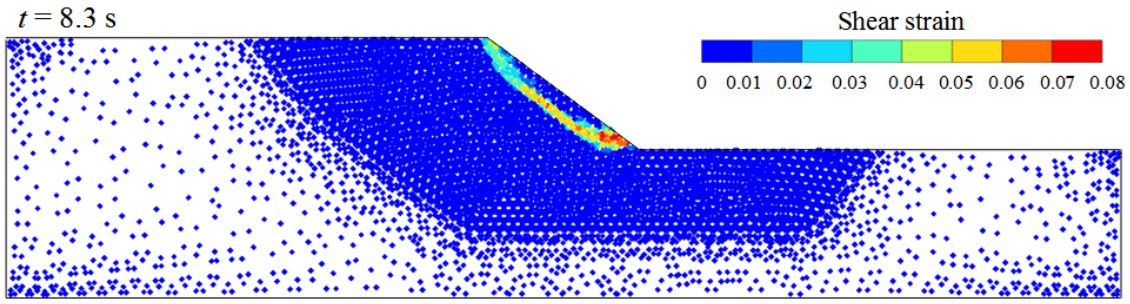

(a)

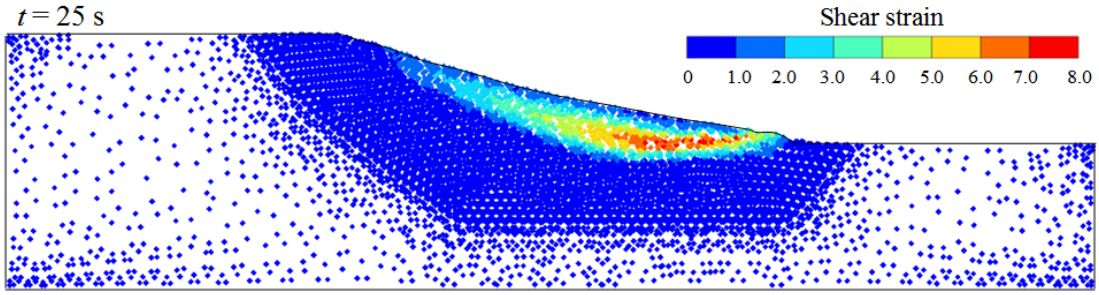

(b)

Fig. 4. Distribution of the shear strain at different times. Note the different scales of the shear strain.

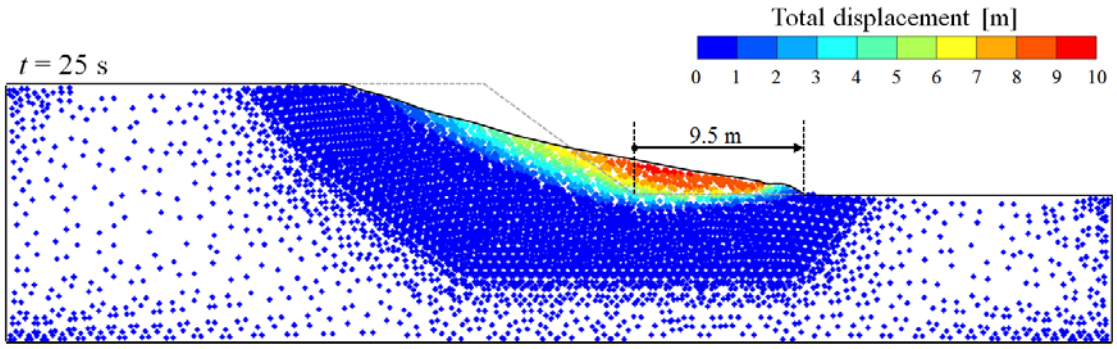

Fig. 5. Distribution of the calculated total displacement at 25 s after the initiation of the failure. The maximum displacement of the toe is also indicated.

Following Skempton [10], a mobilised friction angle (MFA) $\hat{\varphi}'$ is defined as

$$\sin\hat{\varphi}' = \frac{q}{p + (c'/\tan\varphi')} \tag{5}$$

Where q and p' are the deviatoric and effective volumetric stress components defined as follows:

$$q = \frac{\sigma_1' - \sigma_3'}{2} \quad ; \quad p' = \frac{\sigma_1' + \sigma_3'}{2} \tag{6}$$

This measure of the mobilised strength is used to analyse the stress evolution of points

homogeneously distributed along the initial failure surface. Note that $\hat{\varphi}'$ coincides with the peak or residual friction angle values (φ_p', φ_r') when the stress state of such a point is on the peak or residual yield surface envelopes respectively.

A similar analysis of the progressive failure mechanism presented in [31,50] has been carried out. In Fig. 6a the progressive failure phenomenon is represented by plotting the evolution of the MFA (Eq. 5) in 7 material points located along the shear band. It indicates that the degradation of the material initiates at the foot of the slope and propagates upwards.

According to Fig. 6a, it is clear that points along the failure surface reach the peak yield envelope at different moments depending on the evolution of the progressive failure mechanism. Note that time is controlled by the evolution of pore pressures because the internal mechanical transfer of stresses in the slope is an instantaneous process.

In Fig. 6b, the evolution of the progressive failure is represented in terms of the mean mobilised friction angle. It is obtained by averaging the MFA of 20 material points distributed along the initial shear band and it is a measure of the mean mobilised strength in the failure surface. A very similar behaviour was observed in modelling of the Selborne experiment in [31]. Due to the increase of water pressure in the slope induced by the pressure condition imposed along the bottom boundary (see Fig. 3), the mean MFA increases up to a maximum value. Afterwards, there is a drop of the available mobilised strength. Then, the progressive failure develops, maintaining the mean mobilised friction angle approximately constant. This process ends abruptly at t=8.6 s, when the final point in the failure mechanism reaches the peak condition and immediately afterwards it softens down to the residual state. This leads to the onset of instability and the motion begins.

The maximum average mobilized friction angle is attained at t = 8.25 s, when the lower part of the failure surface has already entered into a post-peak strength. This maximum is intermediate between peak and residual strengths and, in the case analyzed, close to the residual value. If a Limit Equilibrium method is used to analyze the slope stability, the maximum calculated at t = 8.25 s is reasonable choice for the soil strength.

Beyond the maximum the average friction decreases somewhat but the process of progressive failure develops at a fairly constant value of the average friction. When the last point in the failure surface reaches peak conditions there is a sudden reduction in average friction and the slope accelerates. This is indicated in Figures 6b and 7a as the “outset of instability”. Up to this time slope displacements are small and unnoticeable at the displacement scale selected to plot Figure 7a.

The behaviour of a material point (P5) is analysed in Fig. 7. Fig. 7a presents the time evolution of the effective cohesion and the displacement experienced by point P5. Fig. 7b shows the stress path of P5. Initially, stress conditions are given by point A in Fig. 7b. The slope remains stable. Due to the increase of pore pressure imposed at the bottom boundary, the effective mean stress clearly decreases. The calculated slight increase of the deviatoric stress is a consequence of the stress redistribution during the initiation of the progressive failure at the toe of the slope. At 8.2 s (indicated by point B in Fig. 7b), this particular material point reaches the peak yield surface. The material point plastifies, triggering a sudden drop of the cohesion (controlled by η), from peak to residual value. At t=8.6 s (the time required to develop the global failure mechanism) the slope becomes unstable and it accelerates. During the instability process, the stresses remain on the residual yield surface despite some numerical oscillations. At t=15 s, after 5 m of displacement, the material point stops when equilibrium has been established for the final geometry. Beyond t=15 s the stress stated of point P5 unloads slightly and enters into the elastic domain.

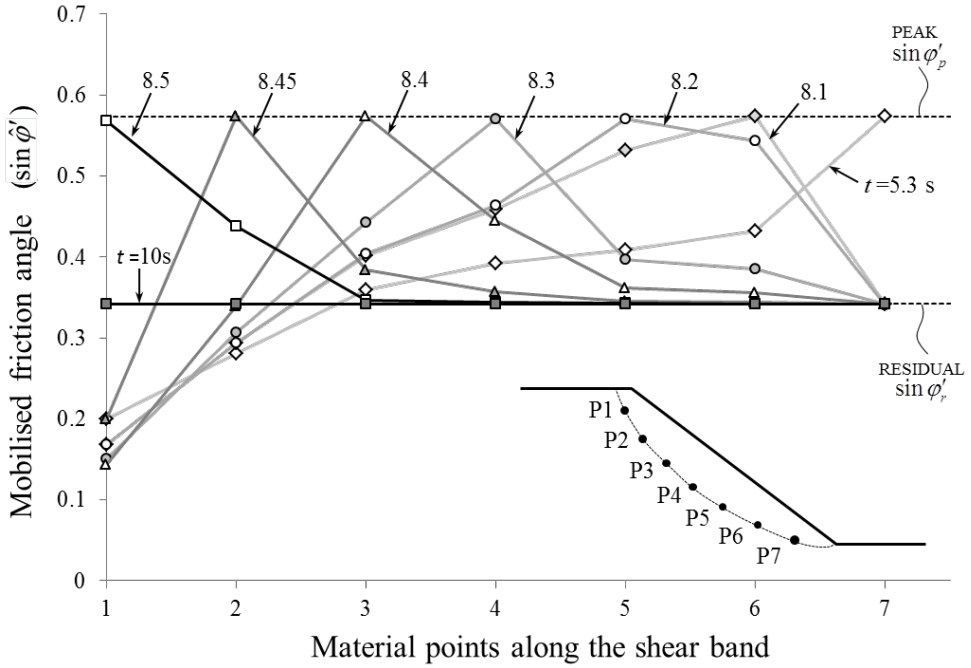

(a)

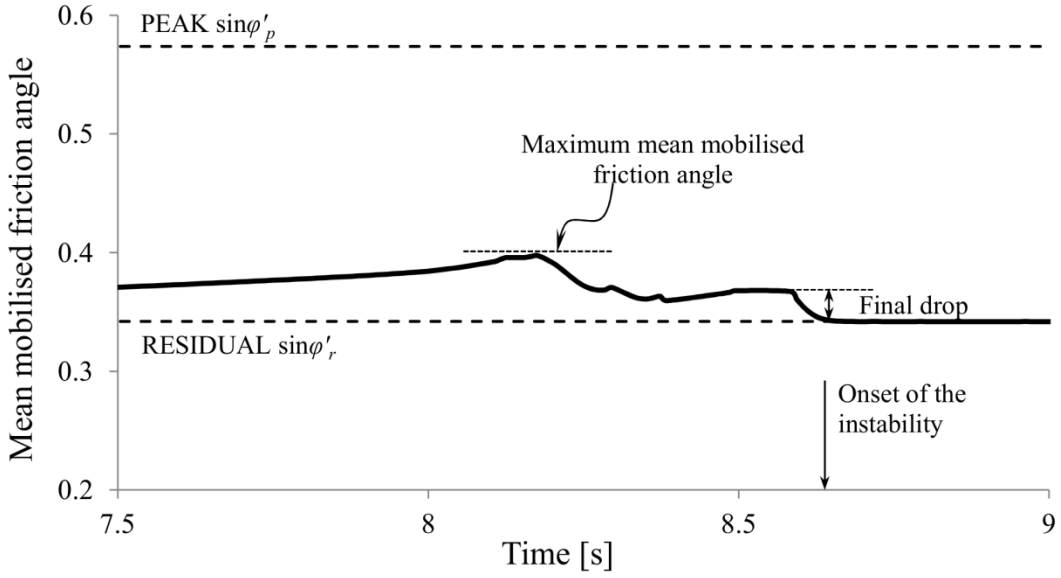

(b)

Fig. 6. (a) Distribution of the mobilised friction angle along the initial shear band at different times. (b) Evolution of progressive failure in terms of mean mobilised friction angle.

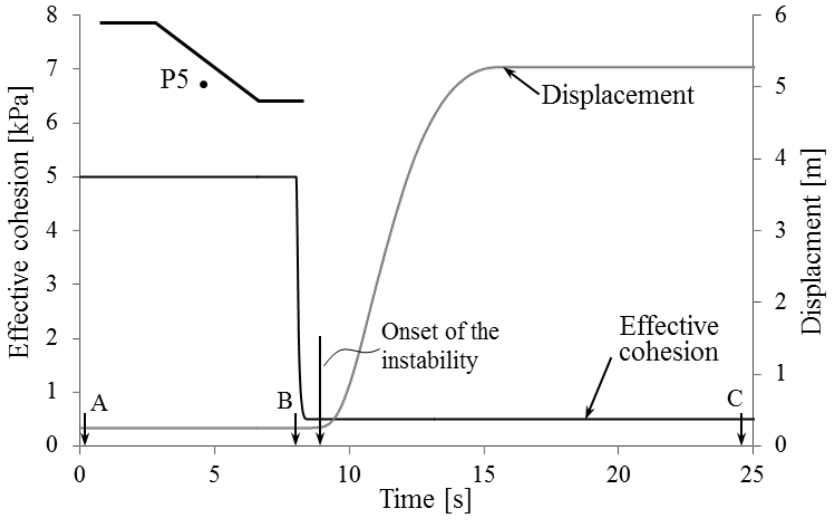

(a)

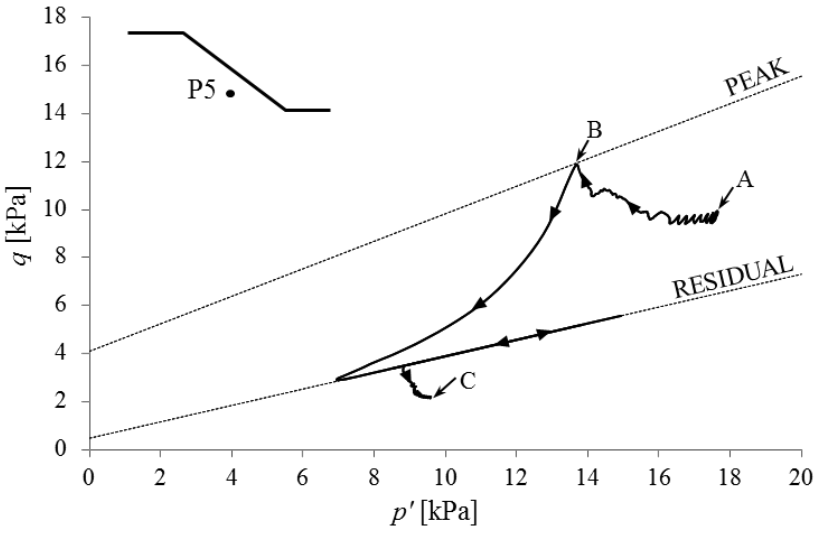

(b)

Fig. 7. Evolution of a material point located on the sliding surface. (a) Effective cohesion and calculated displacement; (b) Stress path in terms of deviatoric stress q and mean effective stress p'.

5 PARAMETRIC STUDY AND RESULTS

A parametric study was carried out with the aim of studying the slope stability and the post-failure behaviour as a function of the soil brittleness.

The brittleness of the soil is defined in terms of the brittleness index (I_B) proposed by Bishop (1967). It is a measure of the decrease of the strength from a peak value (τ_p) to a residual one (τ_r) and it ranges from 0 to 1.

$$I_B = \frac{\tau_p - \tau_r}{\tau_p} \tag{7}$$

where

$$\tau_p = c'_p + \bar{\sigma}'_n \tan \phi'_p \tag{8}$$

$$\tau_r = c'_r + \bar{\sigma}'_n \tan \phi'_r \tag{9}$$

Being $\bar{\sigma}'_n$ the average of the normal stresses to the sliding surface distributed along the initial failure mechanism at the moment in which the global failure develops. This means that I_B is not a local parameter but it is a global measure of the material brittleness, and therefore, a representative value of I_B can be calculated for each simulation that becomes unstable. For stable slopes in which a sliding surface cannot be defined, it is not possible to determine I_B.

A total of 82 simulations have been calculated considering different values of peak and residual strengths. The initial geometry is the same for all of them and it is identical to the case described

previously. Two different maximum excess pore pressures (ΔP) were introduced at the lower boundary, 40 and 70 kPa, to examine the effect of the destabilizing action on the slide run-out and velocity. Common material properties were given in Table 1. The strength parameters that vary for each particular case are indicated in Tables 2 and 3. Note that the selection of the strength values is not intended to strictly represent a certain type of soil but a strain softening material.

In order to evaluate the post-failure slope response, the run-out is an important parameter to determine. Published data on run-out, based on simple approaches, consider a landslide represented by the centre of mass of the total mobilised volume, hence the run-out calculated in those cases is considered as the movement of such a point [51–53]. However, these models do not consider the changes in geometry that may experience the moving mass during the instability.

In this paper, run-out is defined as the distance between the toe of the initial slope and the toe of the slope after failure once equilibrium has been re-established. This is a convenient parameter to evaluate the extent of the slide and it is directly related with the associated risk. It is important to highlight that this definition is not necessarily equivalent to the maximum displacement achieved by any point of the slope.

5.1 *Common peak strength and varying residual friction*

Accepting a common peak envelope defined by c_p'=5 kPa and φ_p'=35º, 61 simulations have been carried out in order to study the effect of residual strength on the onset of instability and post-failure behaviour. A list of these numerical simulations is presented in Table 2, in which values of I_B and run-out are also indicated.

A comparison between initial failure mechanisms obtained with MPM and with a Limit Equilibrium Method LEM (Morgensten-Price) is shown in Fig. 8. The shape of the failure surfaces is very similar to LEM prediction when considering peak strength values. However, the depth of the failure surface slightly depends on the case simulated, ie.: the higher c_r', the deeper the failure surface. More will be said below on the appropriate value of strength parameters to be used in LEM in the case of brittle soils.

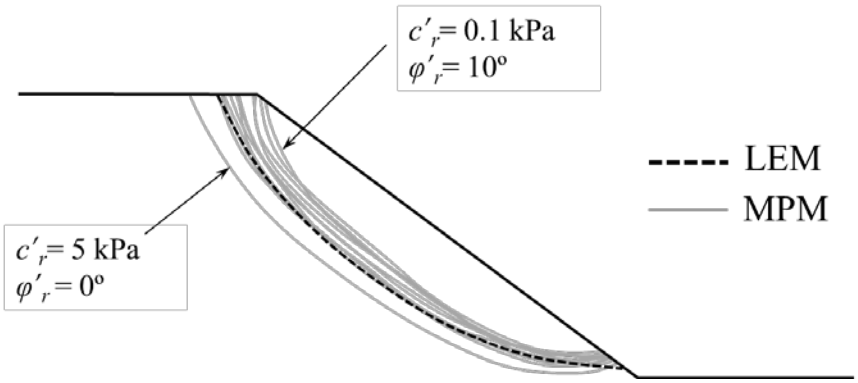

Fig. 8. Comparison between the initial failure mechanisms obtained using MPM and LEM analysis.

Fig. 9a shows the correlation between run-out and I_B. The results converge in a unique curve which indicates that run-out increases with I_B. Note that the maximum run-out observed in this parametric analysis is limited by the right boundary of the computational domain (Fig. 3). Therefore, the maximum run-out calculated is 26 m. Moreover, when I_B >0.75, mobilised material points abandon the dense computational mesh and enter into a rougher mesh (Fig. 3). In these cases the integration becomes less accurate and results may be slightly less reliable.

If the maximum displacement achieved by a point of the slope is considered as a suitable indication of the slide displacement instead of the defined run-out, a similar trend of results is observed in Fig. 9b. However the dispersion is significantly higher in this case.

Note that different values of pore water pressure increase (ΔP) lead to the same I_B-run-out relationship (Fig. 9a). However, the minimum brittleness index required to induce instability ($\hat{I}_B$) varies with ΔP. If ΔP=40 kPa, $\hat{I}_B$ is around 0.5 ($\hat{I}_B^{40}$), whereas for ΔP=70 kPa it decreases to 0.22 ($\hat{I}_B^{70}$). The higher the intensity of the triggering mechanism the lower the I_B to induce instability.

Fig. 10 shows the final geometries of two simulations characterised by the same value of I_B. Despite having a similar value of the run-out (14 m), the maximum displacements are very different (9 and 13 m) as well as the distribution of final displacements. Materials having a low residual cohesion c_r' lead to shallow failures (Fig. 10b), while higher residual cohesion results in a deeper failure and a rotational pattern (Fig. 10a).

Table 2. Run-out and I_B for all simulations performed with a common peak strength envelope (c_p'=5kPa and φ_p'=35º) for different residual strengths and two water pressure recharges (ΔP).

		c_p'=5kPa φ_p'=35º			
		ΔP=40 kPa		ΔP=70 kPa	
c_r' [kPa]	φ_r'[º]	I_B	Run-out [m]	I_B	Run-out [m]
5	35	stable	0.0	stable	0.0
5	25	stable	0.0	stable	0.0

5	20			0.32	1.4
5	15	stable	0.0	0.43	3.4
5	10			0.54	6
5	5	stable	0.0	0.63	11.6
5	0	0.68	14.5		
4	30			stable	0.0
4	25			0.28	1.45
4	20			0.39	2.8
4	15			0.48	5.2
2.5	35	stable	0.0	0.22	0.7
2.5	30			0.33	2.25
2.5	25			0.41	3.35
2.5	20	stable	0.0	0.49	5.26
2.5	15	0.57	6.9	0.57	8.25
2.5	10	0.66	12.1	0.67	12.7
2.5	5	0.74	14.9	0.75	17
2.5	0	0.83	25	0.87	21.1
1.5	30			0.37	2.92
1.5	25			0.46	4.86
1.5	20			0.56	6.45
1.5	15			0.64	10
1.5	10			0.73	14.6
1.2	25	stable	0.0	0.5	5.7
1.2	20	0.58	7	0.6	7.5
1.2	15	0.67	11.2	0.67	11.7
1.2	10	0.75	14.8	0.75	15.6
0.5	35	stable	0.0	0.39	3.5
0.5	30	stable	0.0	0.45	5.4
0.5	25	0.58	7	0.55	6.5
0.5	20	0.65	9.5	0.63	8.9
0.5	15	0.72	14	0.7	13.01
0.5	10	0.8	20	0.79	17.5
0.1	35	stable	0.0		
0.1	30	0.52	6		
0.1	25	0.62	8.8		
0.1	20	0.68	12.6		
0.1	15	0.76	17.4		
0.1	10	0.83	26		
0.1	5	0.91	26		

Fig. 11 illustrates the final geometries after failure for 5 simulations with the same c_r'= 0.5 kPa. The same pattern of displacements is observed in all cases. However, the run-out increases and the slope becomes flatter with increasing values of brittleness.

In order to highlight the dynamics of the failure, Fig. 12 shows the evolution of the displacement (Fig. 12a) and the velocity (Fig. 12b) of a material point initially located just above the initial shear band. These results correspond to the unstable simulations presented previously in Fig. 11. These plots illustrate different phases of an instability process.

The patterns of displacements, after a sliding mechanism was fully developed, follow the description given when interpreting Figures 6 and 7a. Figure 12a shows the effect of I_B on displacements of point P, located at the lower part of the slope. Velocities are also given in Figure 12b. The slide accelerates, reaches a maximum velocity and moves forward towards a new stable profile.

Additionally it can be observed that in slopes exhibiting larger values of I_B, for the same peak strength: (1) the instability occurs earlier; (2) the velocity increases more suddenly; (3) the peak velocities reach higher values; (4) more time is required to reach the final position at rest; and (5) the run-out is longer.

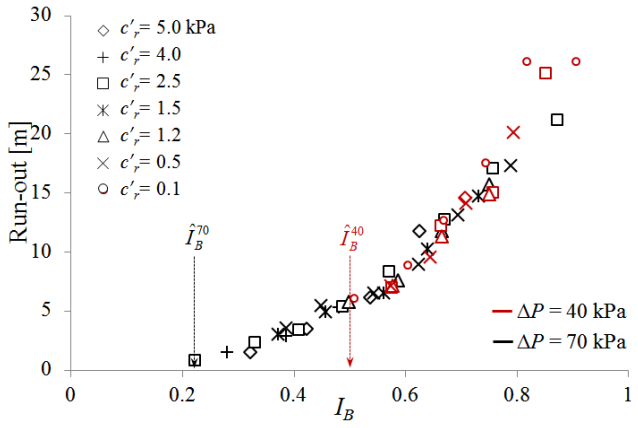

(a)

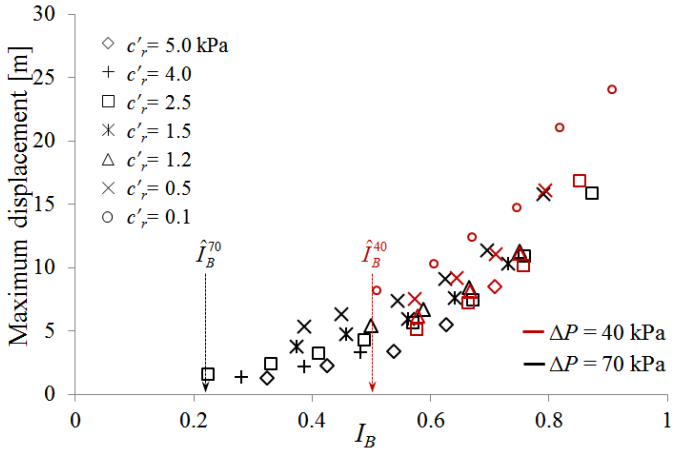

(b)

Fig. 9. (a) Relationship between run-out and I_B. (b) Relationship between maximum displacement achieved by a point and I_B. All simulations have the same peak strength (c_p'=5 kPa and φ_p'=35°). ΔP indicates the imposed pore water pressure which induced the failure.

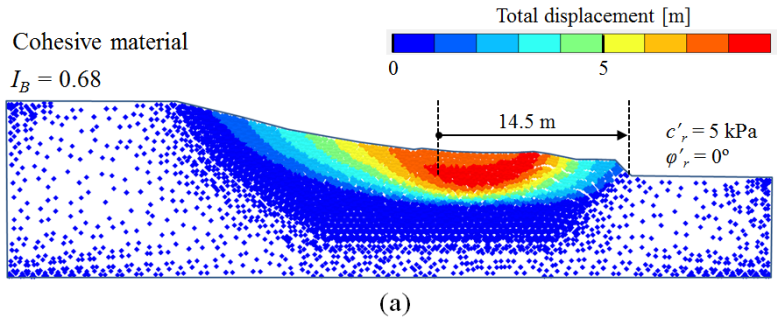

Fig. 10. Final geometry for two simulations with same I_B. The displacements of the material points are indicated in the colour scales. Also indicated is the run-out.

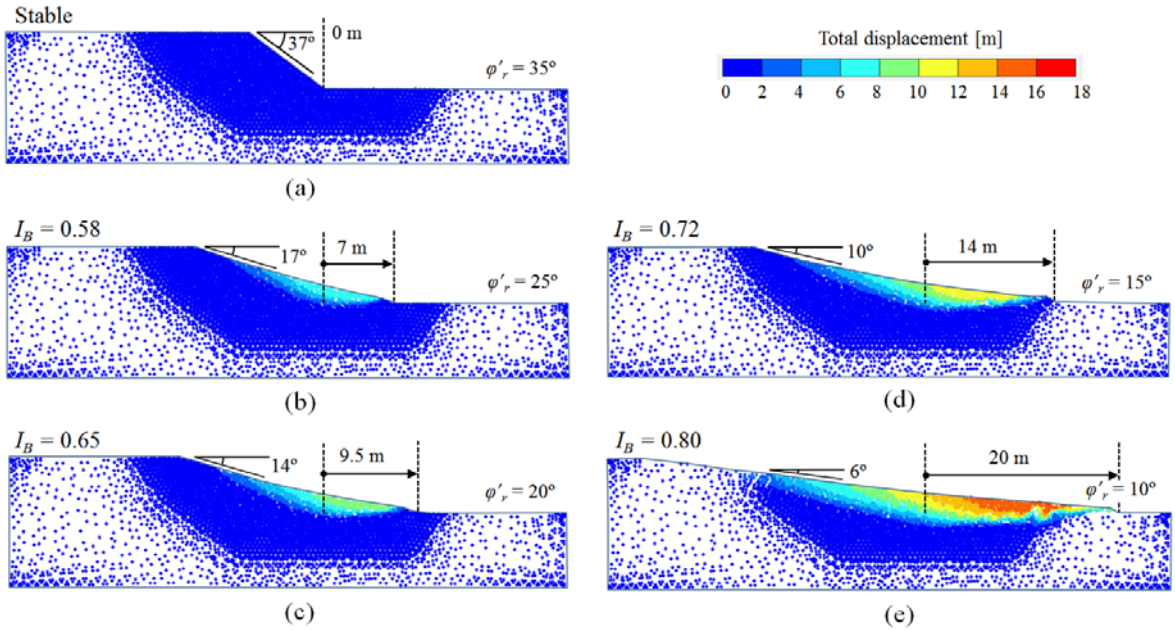

Fig. 11. Final geometries of simulations with c_r'=0.5 kPa. The displacements of the material points are indicated in the indicated colour scale. Also indicated is the run-out.

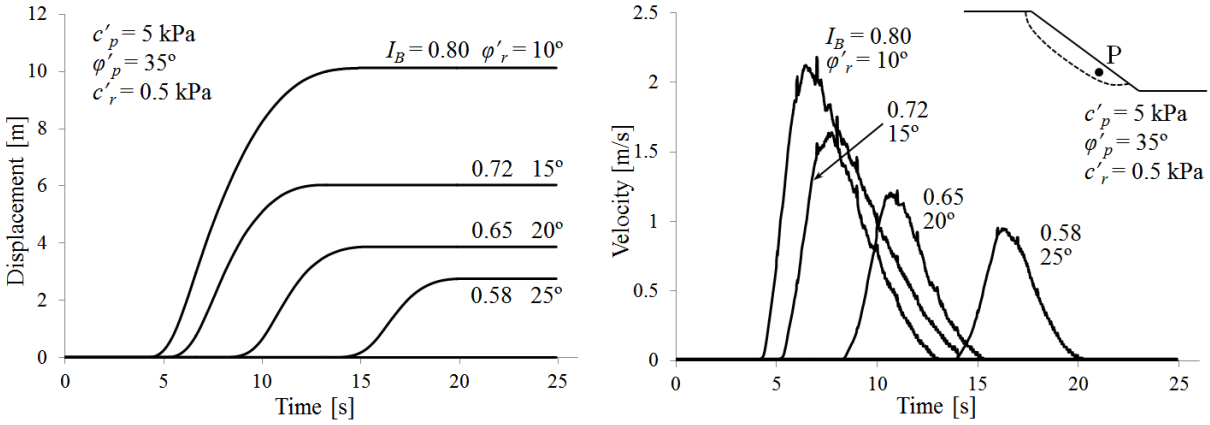

(a) (b)

Fig. 12. (a) Displacement and (b) velocity of the material point P for simulations characterized by c_r'=0.5 kPa.

5.2 *Change in peak strength and varying residual friction*

In the previous Section it was found that a unique relationship developed between run-out and I_B when the peak friction strength envelope was constant (and the residual strength varied in a wide range). The next step was to check if such uniqueness would also hold if peak strength parameters change. In order to explore this scenario three different peak strength parameters were selected, rather arbitrarily, but always ensuring that the slope would fail under the imposed water pressure increase at the lower boundary (ΔP=70 kPa,):

- c_p'=5 kPa, φ_p'=35º (already analysed in the previous section)
- c_p'=5 kPa, φ_p'=45º
- c_p'=9 kPa, φ_p'=20º

For each case, several simulations have been carried out varying the residual strength parameters according to Table 3.

Following the procedure described previously, the brittleness index I_B has been calculated for each unstable simulation. The effect of I_B on run-out is presented in Fig. 13a. Although it is clear that the run-out increases for increasing I_B, two different relationships can be distinguished. Whereas the combination of c_p'=5 kPa and φ_p'=45º matches with the correlation defined in Fig. 9a, those simulations with c_p'=9 kPa and φ_p'=20º define higher run-outs. Fig. 13b shows the variation of the maximum displacement achieved by a point depending on I_B, and, as shown in Fig. 9b, the scatter increases especially for higher values of I_B.

Since the obtained I_B-run-out relationship (Fig. 13) is not unique, three simulations with different peak strengths and the same I_B are analysed in detail (Figs. 14 and 15). The evolution of strain contours (Fig. 14) indicates that the shear strains localise along a single band in the first two simulations (Figs. 14a and 14b). By contrast, a deeper mechanism is developed in the

third simulation (Fig. 14c) which is characterized by a higher cohesion and a lower friction angle with respect to the other two cases. A deeper seated failure involves a larger volume of the mobilized mass and also a longer length of the sliding surface. It seems that the I_B-run-out relationship is also dependent on the failure mechanism. Final displacement fields are given in Fig. 15. Note that values of run-out and maximum displacements are different.

Table 3. Run-out and I_B for all simulations performed with three peak yield surface envelopes.

		ΔP=70 kPa					
		c_p'=5 kPa φ_p'=35º		c_p'=5 kPa φ_p'=45º		c_p'=9 kPa φ_p'=20º	
c_r' [kPa]	φ_r'[º]	I_B	Run-out [m]	I_B	Run-out [m]	I_B	Run-out [m]
6	20					stable	0.0
6	15					0.3	1.45
6	10					0.42	4.8
6	5					0.56	13.41
5	35	stable	0.0				
5	25	stable	0.0				
5	20	0.32	1.4			0.25	1.3
5	15	0.43	3.4			0.36	3
5	10	0.54	6			0.48	8.7
5	5	0.63	11.6			0.63	15
5	0						
4	30	stable	0.0				
4	25	0.28	1.45				
4	20	0.39	2.8				
4	15	0.48	5.2				
2.5	35	0.22	0.7				
2.5	30	0.33	2.25				
2.5	25	0.41	3.35				
2.5	20	0.49	5.26			0.38	5.37
2.5	15	0.57	8.25			0.5	9
2.5	10	0.67	12.7			0.63	13.9
2.5	5	0.75	17				
2.5	0	0.87	21.1				
1.5	30	0.37	2.92				
1.5	25	0.46	4.86				
1.5	20	0.56	6.45	0.65	9.3	0.46	8
1.5	15	0.64	10			0.57	12.55
1.5	10	0.73	14.6			0.68	17.02
1.2	25	0.5	5.7				
1.2	20	0.6	7.5				
1.2	15	0.67	11.7				
1.2	10	0.75	15.6				
0.5	35	0.39	3.5				
0.5	30	0.45	5.4				
0.5	25	0.55	6.5	0.65	10		
0.5	20	0.63	8.9	0.7	13.1	0.52	12.7
0.5	15	0.7	13.01	0.77	15.4	0.61	15.07
0.5	10	0.79	17.5	0.84	19.5		

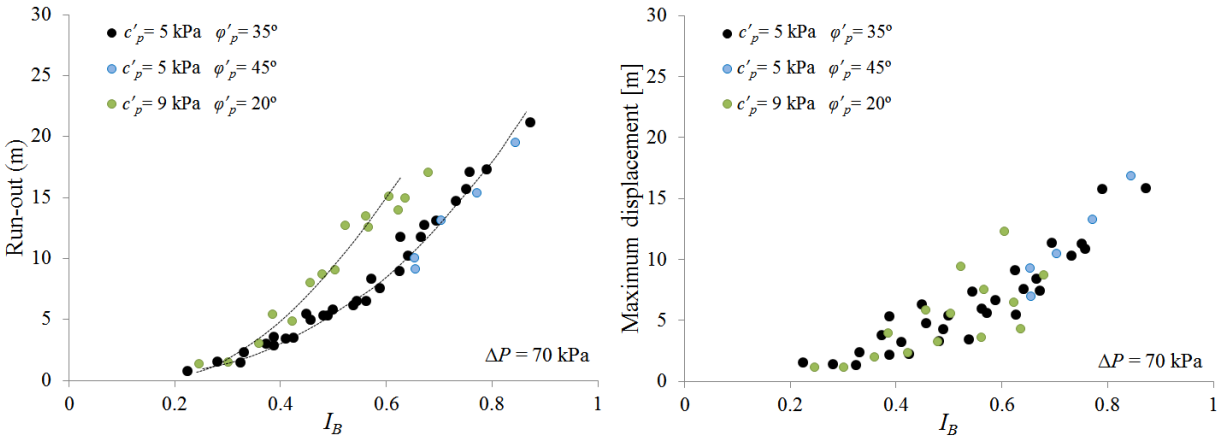

(a) (b)

Fig. 13. Relationships between I_B and (a) run-out and (b) maximum displacement achieved by a point.

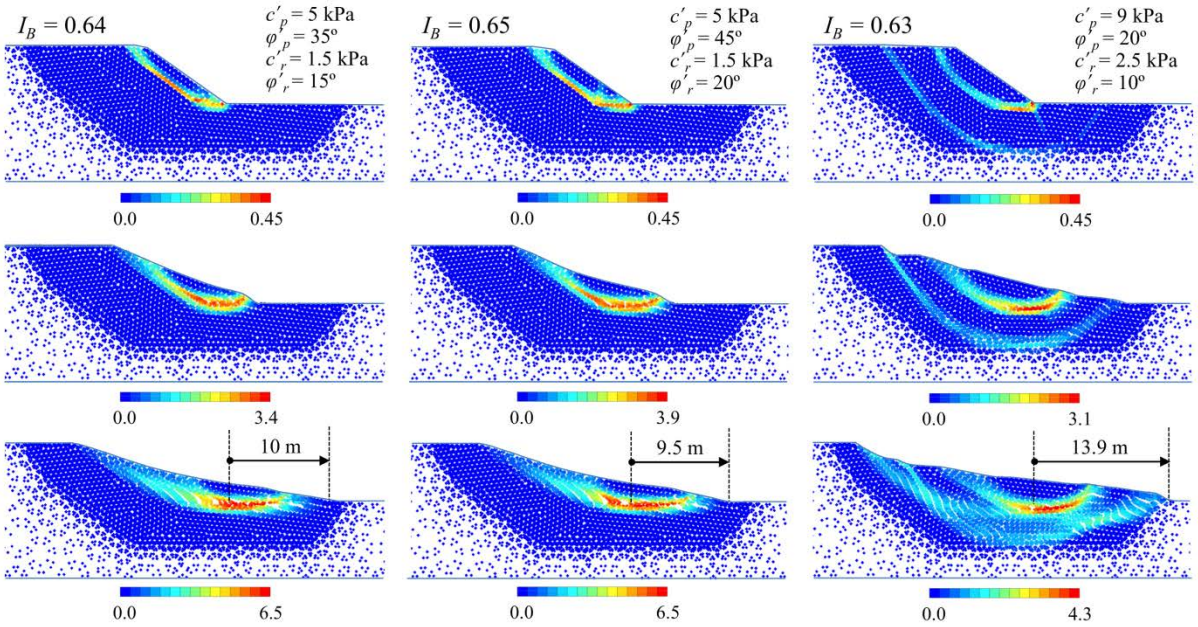

(a) (b) (c)

Fig. 14. Distribution of the shear strain at three different times (the initiation of failure mechanism, an intermediate time, and final geometry) for three simulations with similar I_B but different peak strength envelopes.(a) c_p'=5 kPa, φ_p'=35°; (b) c_p'=5 kPa; φ_p'=45°; (c) c_p'=9 kPa, φ_p'=20°.

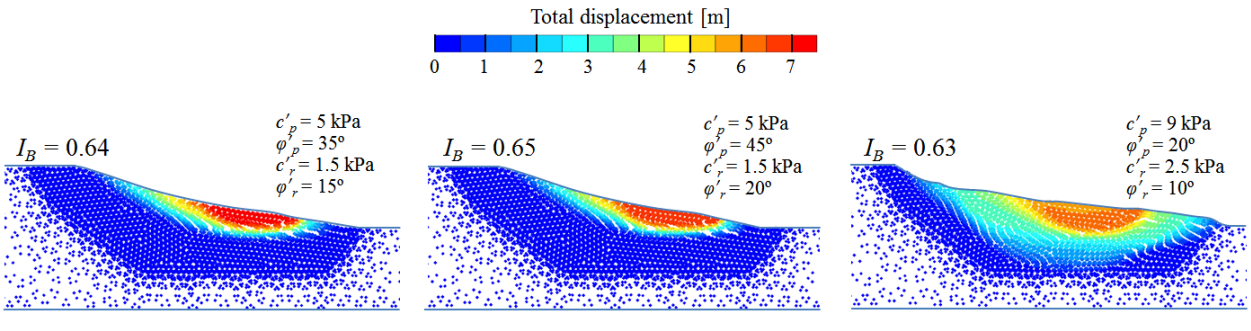

(a) (b) (c)

Fig. 15. Final distribution of total displacements field for 3 cases with similar I_B but different peak strengths. (a) c_p'=5 kPa, φ_p'=35º; (b) c_p'=5 kPa, φ_p'=45º; (c) c_p'=9 kPa, φ_p'=20º.

5.3 *Effect of cohesion and friction angle decrease in the onset of failure*

The onset of failure is analysed depending on the cohesion and friction decrease (Eqs. (10) and (11) respectively) and on the external triggering action (pore water pressure increase in the lower boundary ΔP). Consider the following "brittleness" ratios for effective cohesion and friction:

$$dc' = \left(c'_p - c'_r\right) \Big/ c'_p \tag{10}$$

$$d\varphi' = \left(\tan\varphi'_p - \tan\varphi'_r\right) \Big/ \tan\varphi'_p \tag{11}$$

Zero values of these indices corresponds to a ductile behaviour whereas a unit value represents a highly brittle response.

All the combinations of dc' and $d\varphi'$ shown in Table 2 for ΔP =40 kPa and ΔP=70 kPa are shown in Fig. 16. It is clear that the lower the increments of water pressure, the higher is the required strength reduction to make the slope unstable. For instance, in the case of ΔP =40 kPa, in order to reach failure, the soil should exhibit a full brittleness in one of the strength parameters and a full ductility in the other, or the combination given by the threshold straight line separating failure from stability.

These results suggest that both cohesion and friction angle play a similar role in determining a threshold that define whether the slope will become unstable, or on the contrary, will remain stable.

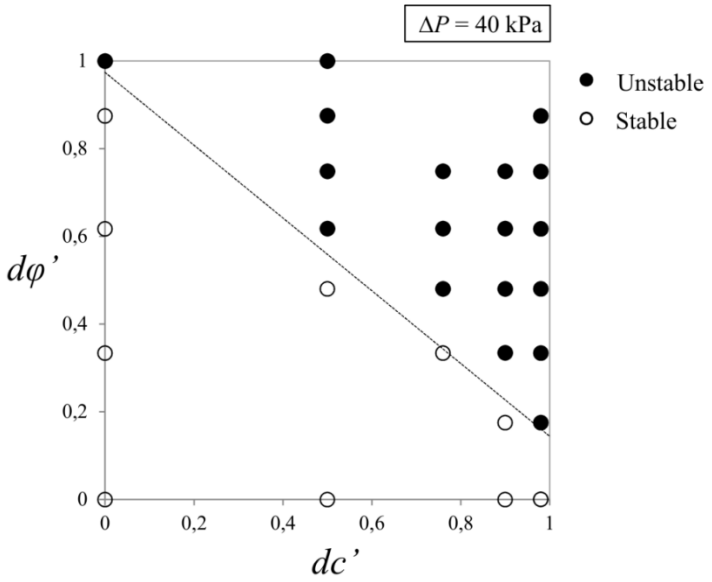

(a)

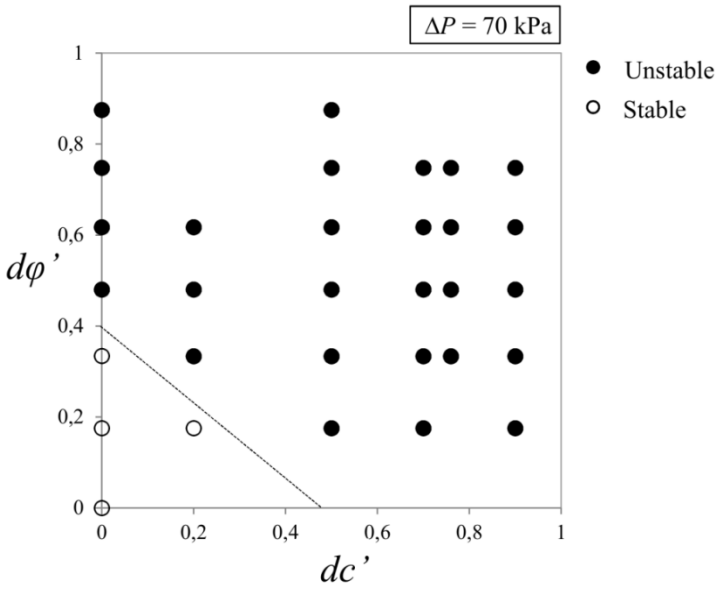

(b)

Fig. 16. Stability of the slope depending on the combination of cohesion drop (dc') and friction angle decrease ($d\varphi'$). The increase of pore pressure at at the lower boundary is (a) ΔP =40 kPa and (b) ΔP=70 kPa. The same peak strength is maintained in all these simulations (c_p'=5 kPa and φ_p'=35º).

5.4 *Effect of peak and residual strength in run-out*

In previous sections, the I_B-run-out relationship is analysed but the relevance of peak and residual strength is not discussed. This is because I_B combines both effects in a single parameter.

The influence of peak and residual strengths on the value of run-out is shown in Fig. 17. It is clear that simulations having the same residual strength have quite similar values of run-out even if different peak yield surface envelopes define the material (Fig. 17).

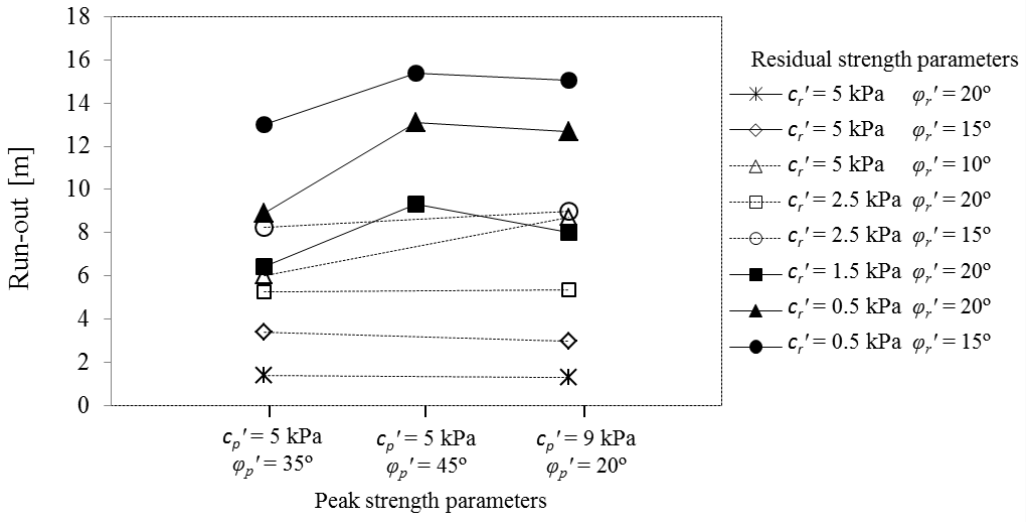

Fig. 17. Influence of residual strength on run-out for three different peak Mohr-Coulomb envelopes.

6 DISCUSSION

6.1 *Run-out vs maximum displacement*

It has been shown that run-out, defined as the distance between the toe of the initial slope and the toe once equilibrium has been re-established after the instability, is not equivalent to the maximum displacement achieved by any point of the slope (see Figs. 9 and 13). While a clear relationship cannot be obtained between I_B and maximum displacement, I_B and run-out correlate well.

The difference between run-out and maximum displacement is evident especially when the failure mechanism is deep and the landslide is essentially a rotational movement (Fig. 10a). The deeper the failure surface (cohesive component of strength dominates) the larger the ratio between run-out and maximum point displacements. However, both lengths are similar when the initial failure is shallow (Fig. 10b).

6.2 *Effect of peak and residual strength in the whole instability process*

Here the role played by peak and residual strengths in the stability of the slope, in the slip surface geometry and in the post-failure response is discussed.

According to the results presented in Fig. 6, it is clear that the peak envelope controls the initiation of the progressive failure because it determines when the first point reaches the maximum strength. However, the redistribution of stresses due to the strain softening of the material and the propagation of the progressive failure is a complex process governed by both peak and residual states. Note that the mean mobilised strength in the slope (Fig. 6b) remains always below the peak value.

In agreement with this, it has been observed that the geometry of the failure mechanism is definitely influenced by both peak and residual strengths (Figs. 8 and 14) but peak strength has a stronger effect. Especially the peak cohesion highly influences the depth of the mechanism.

Finally, the run-out is essentially influenced by the residual state (Fig. 17). It makes sense because when the post-failure stage initiates the soil in the shear band has experienced enough plastic shear strain to be totally softened. This behaviour is also shown in Fig. 6b.

6.3 *Residual cohesion in brittle soils*

In brittle soils, peak friction angles may take values ranging from 5º to 45º depending on the type of soil. The variability of peak cohesion can be also very large (from 0 kPa to more than,

say, 200 kPa in very stiff clays). However, residual effective cohesion is very low or non-existent.

The selection of peak and strength values presented in the parametric analysis (Section 5) represents a large variability of strain softening materials, and some of them include unlikely values for the residual cohesion (up to 6 kPa).

In order to analyse if this restriction have some effect on the results, an additional figure is included here (Fig. 18) in which only those simulations from Table 3 having a small c_r' (c_r'≤1.5 kPa) are presented. The number of cases in the simulations performed decrease substantially but the relationships between I_B and run-out and maximum displacement look essentially the same as those obtained when interpreting the complete set of simulations (Fig. 13).

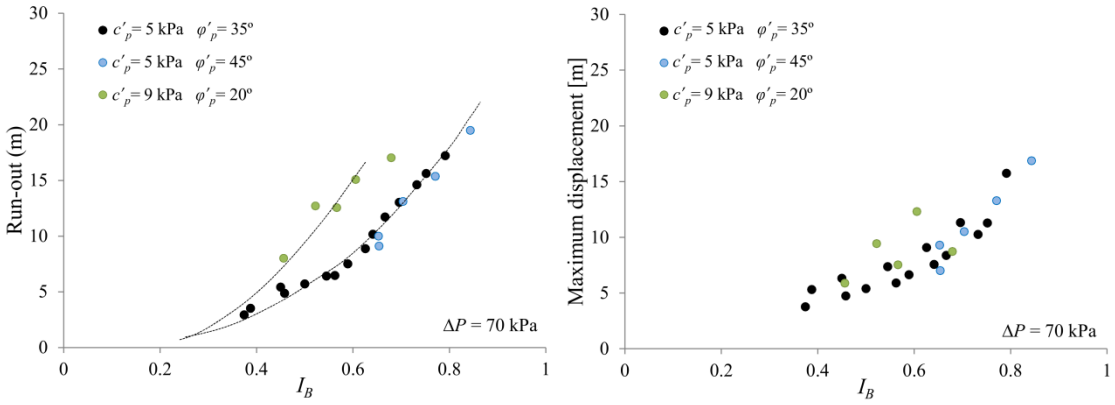

(a) (b)

Fig. 18. Relationships between I_B and (a) run-out and (b) maximum displacement achieved by a point. Cases with c_r'≤ 1.5 kPa.

7 CONCLUSIONS

The stability and post-failure behaviour of a saturated slope have been analysed by means the MPM which has been proved that it is capable to simulate both the initiation of failure, which involves small strains, and the post-failure stage, generally characterised by large displacements. A homogeneous slope with a regular geometry has been analysed. The slope failure is triggered by increasing the water pressure on the lower boundary of the domain.

The slope material has been defined by a strain-softening elastoplastic constitutive law that allows the simulation of the strength decrease (from a peak to a residual value). The progressive failure mechanism, typically observed in brittle materials, is reproduced and analysed. Both, peak and residual values of the strength control the slope failure which progresses from the toe to the crest of the slope. On the contrary, the post-failure behaviour is mainly controlled by the

residual strength and it has an important effect on the run-out. The results show that the geometry of the failure surface determines the final displacement field.

The effect of the material brittleness, defined in terms of brittleness index I_B (proposed by Bishop [12]), on the post-failure behaviour has been identified by means of a parametric analysis combining peak and residual values of cohesion and friction angle. Both run-out and the maximum displacements have been represented in terms of the brittleness index. Run-out was defined here as the distance between the toe of the initial slope and the toe of the slope after failure once equilibrium has been re-established. It was found that run-out increases with I_B and both correlate well when a common peak strength envelope is adopted. On the contrary, a clear relationship has not been obtained between I_B and maximum displacement.

The onset of failure also depends on the magnitude of the triggering mechanism. The higher the intensity of the triggering mechanism, the lower I_B is sufficient to induce instability. This fact allows defining a brittleness threshold $\hat{I}_B^{\Delta P}$ which determines the minimum brittleness required to induce instability for a certain excess pore pressure. However, the magnitude of the applied excess pressure (ΔP) does not change the general observations discussed above.

8 ACKNOWLEGDMENTS

The software used in this work is a version of the MPM code developed by the MPM Research Community formed by 6 partners: Deltares (The Netherlands), Universitat Politècnica de Catalunya (Spain), University of Cambridge (UK), Technische Universität Hamburg-Harburg (Germany), Università degli Studi di Padova (Italy), and Delft University of Technology (The Netherlands).

9 REFERENCES

[1] Fell R, Hungr O, Leroueil S, Riemer W. Keynote lecture - Geotechnical engineering of the stability of natural slopes, and cuts and fills in soil. ISRM Int. Symp., Melbourne, Australia: International Society for Rock Mechanics; 2000.

[2] Pinyol N, Alonso E, Corominas J, Moya J. Canelles landslide: modelling rapid drawdown and fast potential sliding. Landslides 2012;9:33–51.

[3] Alonso E, Gens A. The landslide of Cortes de Pallas, Spain. Géotechnique 1993;43:507–21.

[4] Ganerød G, Grøneng G, Rønning J, Dalsegg E, Elvebakk H, Tønnesen J, et al. Geological model of the Åknes rockslide, western Norway. Eng Geol 2008;102:1–18.

[5] Qi S, Yan F, Wang S, Xu R. Characteristics, mechanism and development tendency of deformation of Maoping landslide after commission of Geheyan reservoir on the Qingjiang River, Hubei Province, China. Eng Geol 2006;86:37–51.

[6] Alcantara-Ayala I, Dominguez-Morales L. The San Juan de Grijalva catastrophic

landslide, Chiapas, Mexico: lessons learnt. In: Casagli N, Fanti R, Tofani V, editors. Web Proc. First World Landslide Forum. Int. Consort. Landslides. United Nations Int. Strateg. Disaster Reductions, Tokyo, Japan: 2008, p. 96–9.

[7] Wang F, Zhang Y, Huo A, Matsumoto T, Huang B. The July 14, 2003 Qianjiangping landslide, Three Gorges Reservoir, China. Landslides 2004;1:157–62.

[8] Terzaghi K, Peck R. Soil mechanics in engineering practice. New York: Wiley; 1948.

[9] Taylor DW. Fundamentals of soil mechanics. New York: Wiley; 1948.

[10] Skempton AW. Fourth Rankine Lecture: Long-term stability of clay slopes. Géotechnique 1964;14:77–102.

[11] Bjerrum L. Progressive failure in slopes in overconsolidated plastic clays and clay shales. J Soil Mech Found Div 1967;93:3–49.

[12] Bishop AW. Progressive failure-with special reference to the mechanism causing it. Proc. Geotech. Conf., vol. 2, Oslo: 1967, p. 142–50.

[13] Palmer C, Rice JR. The growth of slip surfaces in the progressive failure of overconsolidated clay. Proc R Soc A 1973;332:527–48.

[14] Stark TD, Eid HT. Slope stability analyses in stiff fissured clays. J Geotech Geoenv Engng 1994;123:335–43.

[15] Puzrin AM, Germanovich LN. The growth of shear bands in the catastrophic failure of soils. Proc R Soc A Math Phys Eng Sci 2005;461:1199–228. doi:10.1098/rspa.2004.1378.

[16] Yamaguchi H, Kimura T, Fuji-I N. On the influence of pregressive failures on the bearing capacity of shallow foundations in dense sand. Soils Found 1976;16:11–22.

[17] Potts DM, Dounias GT, R. VP. Finite element analysis of progressive failure of Carsington embankment. Géotechnique 1990;40:79–101.

[18] Potts D, Kovacevic N, Vaughan P. Delayed collapse of cut slopes in stiff clay. Géotechnique 1997;47:953–82.

[19] Gens A, Alonso EE. Aznalcóllar dam failure. Part 2: Stability conditions and failure. Geotechnique 2006;56:185–201.

[20] Zabala F, Alonso EE. Progressive failure of Aznalcóllar dam using the material point method. Géotechnique 2011;61:795–808. doi:10.1680/geot.9.P.134.

[21] Troncone A. Numerical analysis of a landslide in soils with strain-softening behaviour. Geotechnique 2005;55:585–96.

[22] Troncone A, Conte E, Donato A. Two and three-dimensional numerical analysis of the progressive failure that occurred in an excavation-induced landslide. Eng Geol 2014;183:265–75. doi:10.1016/j.enggeo.2014.08.027.

[23] Alonso EE, Pinyol NM. Slope stability in slightly fissured claystones and marls. Landslides 2014. doi:10.1007/s10346-014-0526-5.

[24] Soga K, Alonso E, Yerro A, Kumar K, Bandara S. Trends in large-deformation analysis of landslide mass movements with particular emphasis on the material point method. Géotechnique 2015. doi:http://dx.doi.org/10.1680/jgeot.15.LM.005.

[25] Sulsky D, Zhou S-J, Schreyer HL. Application of a particle-in-cell method to solid mechanics. Comput Phys Commun 1995;87:236–52. doi:10.1016/0010-4655(94)00170-7.

[26] Beuth L, Wieckowski Z, Vermeer PA. Solution of quasi-□static large-□strain problems by the material point method. Int J Numer Anal Methods Geomech 2011;35:1451–65. doi:10.1002/nag.

[27] Jassim I, Stolle D, Vermeer P. Two-□phase dynamic analysis by material point method.

Int J Numer Anal Methods Geomech 2013;37:2502–22. doi:10.1002/nag.

[28] Yerro A, Alonso E, Pinyol N. The material point method for unsaturated soils. Géotechnique 2015;65:201–17. doi:http://dx.doi.org/10.1680/geot.14.P.163.

[29] Hamad F, Stolle D, Vermeer P. Modelling ofmembranes in thematerial point method with applications. Int J Numer Anal Methods Geomech 2015;39:833–53. doi:10.1002/nag.

[30] Conte E, Silvestri F, Troncone A. Stability analysis of slopes in soils with strain-softening behaviour. Comput Geotech 2010;37:710–22.

[31] Alonso E, Yerro A, Pinyol N. Recent developments of the Material Point Method for the simualtion of landslides. Keynote Lect. Int. Symp. Geohazards Geomech., Warwick, UK: 2015.

[32] Cooper M, Bromhead E, Petley D, Grant D. The Selborne cutting stability experiment. Geotechnique 1998;48:83–101.

[33] Sulsky D, Chen Z, Schreyer HL. A particle method for history-dependent materials. Comput Methods Appl Mech Eng 1994;118:179–96. doi:10.1016/0045-7825(94)90112-0.

[34] Sulsky D, Schreyer HL. Axisymmetric form of the material point method with applications to upsetting and Taylor impact problems. Comput Methods Appl Mech Eng 1996;139:409–29. doi:10.1016/S0045-7825(96)01091-2.

[35] Abe K, Soga K, Bandara S. Material point method for coupled hydromechanical problems. J Geotech Geoenvironmental Eng 2014;140:1–16. doi:10.1061/(ASCE)GT.1943-5606.0001011.

[36] Cromer A. Stable solutions using the Euler approximation. Am J Phys 1981;49:455–9.

[37] Cundall PA. Distinct element models of rock and soil structure. In: Brown ET, editor. Anal. Conlputational Methods Eng. Rock Mech., London: Allen and Unwin; 1987, p. 129–63.

[38] Al-Kafaji IKJ. Formulation of a Dynamic Material Point Method (MPM) for Geomechanical Problems. Universität Stuttgart, 2013.

[39] Bardenhagen SG, Kober EM. The generalized interpolation material point method. Comput Model Eng Sci 2004;5:477–95. doi:10.3970/cmes.2004.005.477.

[40] Sadeghirad A, Brannon R, Burghardt J. A convected particle domain interpolation technique to extend applicability of the material point method for problems involving massive deformations. Int J Numer Methods Eng 2011;86:1435–56. doi:10.1002/nme.

[41] Kamojjala K, Brannon R, Sadeghirad A, Guilkey J. Verification tests in solid mechanics. Eng Comput 2013;31:193–213. doi:10.1007/s00366-013-0342-x.

[42] Abbo A, Sloan S. A smooth hyperbolic approximation to the Mohr-Coulomb yield criterion. Comput Struct 1995;54:427–41.

[43] Dounias G, Potts D, Vaughan P. Finite element analysis of progressive failure: two case studies. Comput Geotech 1988;6:155–75.

[44] Potts D, Dounias G, Vaughan P. Finite element analysis of progressive failure of Carsington embankment. Géotechnique 1990;40:79–101.

[45] Dounias G, Potts D, Vaughan P. Analysis of progressive failure and cracking in old British dams. Géotechnique 1996;46:621–40.

[46] Potts D, Zdravkovic L. Finite element analysis in geotechnical engineering: application. London: Thomas Telford; 1999.

[47] Potts D, Kovacevic N, Vaughan P. Delayed collapse of cut slopes in stiff clay. Géotechnique 1997;47:953–82.

[48] Yerro A. MPM modelling of landslides in brittle and unsaturated soils. Universitat Politècninca de Catalunya, 2015.

[49] Rots JG, Nauta P, Kuster GMA, Blaauwendraad J. Smeared Crack Approach and Fracture Localization in Concrete. Heron 1985;30:1–48.

[50] Yerro A, Alonso E, Pinyol N. Modelling progressive failure with MPM. In: Hicks M, Brinkgreve RBJ, Rohe A, editors. Numer. Methods Geotech. Eng., 214 Taylor & Francis Group; 2014, p. 319–23.

[51] Scheidegger AE. On the prediction of the reach and velocity of catastrophic landslides. Rock Mech 1973;5:231–6.

[52] Hsü KJ. Catastrophic debris streams generated by rockfalls. Geol Soc Am Bull 1975;86:129–40.

[53] Sassa K. Special lecture: Geotechnical model for the motion of landslides. In: Bonnard C, editor. Proc. 5th Symp. Landslides, vol. 1, Rotterdam: Balkema; 1988, p. 37–55.